Kim Y, Chang D, Kim J *et al.* Gallbladder removal simulation for laparoscopic surgery training: A hybrid modeling method. JOURNAL OF COMPUTER SCIENCE AND TECHNOLOGY 28(3): 499–507 May 2013. DOI 10.1007/s11390-013-1351-3

Gallbladder Removal Simulation for Laparoscopic Surgery Training: A Hybrid Modeling Method

Youngjun Kim[1], Dongjune Chang[2], Jungsik Kim[2], and Sehyung Park[1]

[1] *Center for Bionics, Korea Institute of Science and Technology, Seoul 136-791, Korea*

[2] *Department of Mechanical Engineering, Korea Advanced Institute of Science and Technology, Daejeon 305-701, Korea*

E-mail: junekim@kist.re.kr; {dongjune.chang, jungkim}@kaist.ac.kr; sehyung@kist.re.kr

Received March 29, 2012; revised July 2, 2012.

Abstract Laparoscopic surgery has many advantages, but it is difficult for a surgeon to achieve the necessary surgical skills. Recently, virtual training simulations have been gaining interest because they can provide a safe and efficient learning environment for medical students and novice surgeons. In this paper, we present a hybrid modeling method for simulating gallbladder removal that uses both the boundary element method (BEM) and the finite element method (FEM). Each modeling method is applied according to the deformable properties of human organs: BEM for the liver and FEM for the gallbladder. Connective tissues between the liver and the gallbladder are also included in the surgical simulation. Deformations in the liver and the gallbladder models are transferred via connective tissue springs using a mass-spring method. Special effects and techniques are developed to achieve realistic simulations, and the software is integrated into a custom-designed haptic interface device. Various computer graphical techniques are also applied in the virtual gallbladder removal laparoscopic surgery training. The detailed techniques and the results of the simulations are described in this paper.

Keywords deformable body modeling, gallbladder removal, laparoscopic surgery, training simulation

1 Introduction

Minimally invasive surgery (MIS) is currently a widely used approach for shortening recovery time and reducing patient pain. Laparoscopic surgery is one of the most successful applications of MIS, but unfortunately, the required surgical skills are difficult to acquire. Unlike traditional invasive surgery, problems arise in laparoscopic surgery due to a narrow field of vision and a weak feeling of contact, as well as the pivoting motions of the long surgical instruments that surgeons manipulate while watching 2D images from a laparoscope. Animal experiments and patient trials have been carried out in the past but were difficult due to issues regarding cost and safety. Because of these drawbacks, several virtual simulators have been developed to provide laparoscopic surgery training by virtually reproducing the surgical procedures[①~④]. These allow medical students and novice surgeons to be trained in a safe and reproducible learning environment.

1.1 Laparoscopic Gallbladder Removal

Gallbladder removal (or cholecystectomy) is an operation performed to remove the gallbladder from the liver. When a patient has gallstones or other gallbladder dysfunction, this surgery may be performed. Recently, traditional open surgery for gallbladder removal has been replaced by laparoscopic surgery in many cases. Typical laparoscopic surgery procedures are as follows[⑤]: 1) injection of CO_2 gas into the abdomen, 2) retraction of the liver to secure a clear view, 3) clamping the biliary tract, 4) cutting the biliary tract, 5) dissecting the gallbladder by cauterizing connective tissues between the gallbladder and the liver, and 6) removing the gallbladder from the body through the umbili-

Regular Paper

This research was supported by the Ministry of Culture, Sports and Tourism and the Korea Creative Content Agency in the Culture Technology Research & Development Program 2009. This research was also supported in part by the Korea Institute of Science and Technology Institutional Program under Grant No. 2E23780.

①SEP. http://www.simsurgery.com/, March 2012.

②LapSim®. http://www.surgical-science.com/, March 2012.

③LAP mentor. http:/simbionix.com/simulators/lap-mentor/, March 2012.

④Laparoscopy™. http://www.immersion.com/, March 2012.

⑤WeBSurg. http://www.websurg.com/, March 2012.

cus. Instruments used for gallbladder removal include graspers, cauterizers, retractors, electric cutters, and electric scissors. In this paper, we focus only on step 5. More specifically, this step involves dissecting the gallbladder from the liver by burning the connective tissues using an electric cauterizer while pulling the gallbladder with graspers. Typically, in this step, graspers are held in the left hand of the surgeon and the cauterizers in the right.

1.2 Related Work

Over the past two decades, many research groups have been investigating virtual medical simulations in which both reality and interactivity play a key role. Simulation Open Framework Architecture (SOFA)⑥,[1] is one of the most sophisticated frameworks available for medical simulation. It consists of a large number of simulation modules such as deformable body modeling, collision detection, mapping, solver for dynamic simulation, and mesh handling components. Studies relating to SOFA can be found in [2-7].

The characteristics of various deformable body modeling methods (e.g., mass-spring model, linked volumes, tensor-mass model, finite element method (FEM), boundary element method (BEM)) have been summarized and compared in the literature[2-3]. However, few studies have focused on gallbladder removal simulation, with the exception of an outdated method that uses deformable splines, proposed by Cover *et al.*[7], and two more recent studies[8-9].

Recently, commercially produced laparoscopic surgery simulators have been introduced on the market. Such simulators include SEP (SimSurgery, Norway)⑦, LapSim (Surgical-Science, Sweden)⑧, LAP Mentor (Simbionix, USA)⑨, and LapVR (Immersion, USA)⑩, among others. Although these systems provide various virtual training solutions, they are limited by their high cost and little fidelity. Moreover, the detailed algorithms behind these systems cannot be found in the literature.

1.3 Proposed Method

In this paper, we propose a novel method that uses a hybrid system for laparoscopic surgery simulation. The proposed simulator adopts the merits of both BEM and FEM models, using BEM for the liver and FEM for the gallbladder. Based on each organ's properties, suitable deformable body modeling methods were chosen. A realistic modeling method for connective tissues is also proposed here, and implementation issues regarding visualization, collision detection, virtual instrument manipulation, and hardware development are described in the following section.

2 Methods

2.1 BEM Liver Modeling

We modeled the deformable characteristics of the liver using BEM[10], an approach widely used in continuum mechanics. The human liver is entirely covered by visceral peritoneum, a thin and double-layered membrane that reduces friction against other organs. From a biomechanical point of view, this membrane consists of many visceral smooth muscles, giving it an elastic quality. We therefore choose to treat this membrane as a thin surface boundary with BEM rather than using a volumetric model in FEM. The BEM computes the unknown variables on the organ's boundary instead of over its entire body. The boundary of the liver is discretized into n elements, and the points representing unknown values, tractions, and displacements are defined as nodes.

The resulting system of equations is given by

$$\boldsymbol{HU} = \boldsymbol{GT}, \tag{1}$$

where $\boldsymbol{H}$ and $\boldsymbol{G}$ are $3n \times 3n$ dense matrices, and $\boldsymbol{U}$ and $\boldsymbol{T}$ are the displacement and traction vectors, respectively. The boundary conditions (i.e., displacements and tractions) are applied at each node to solve these algebraic equations. When the displacement value is given on a node, the traction value can be obtained, and vice versa.

Equation (1) can be rearranged as

$$\boldsymbol{AY} + \overline{\boldsymbol{A}}\,\overline{\boldsymbol{Y}} = 0 \Rightarrow \boldsymbol{Y} = \boldsymbol{A}^{-1}(-\overline{\boldsymbol{A}}\,\overline{\boldsymbol{Y}}), \tag{2}$$

where $\boldsymbol{Y}$ is the vector consisting of unknown boundary conditions, and $\boldsymbol{A}$ and $\overline{\boldsymbol{A}}$ consist of the columns of the $\boldsymbol{H}$ and $\boldsymbol{G}$ matrices that correspond to the indexes of $\boldsymbol{Y}$ and $\overline{\boldsymbol{Y}}$, respectively. $\boldsymbol{Y}$ can be obtained by solving (2).

To achieve a realistic simulation in real time, it is necessary to provide visual and haptic feedback with updating rates greater than 30 Hz and 500 Hz, respectively[11]. Calculating the inverse of $\boldsymbol{A}$, $\boldsymbol{A}^{-1}$, requires a high computational cost; we therefore use a

⑥SOFA. http://www.sofa-framework.org/, March 2012.

⑦SEP. http://www.simsurgery.com/, March 2012.

⑧LapSim®. http://www.surgical-science.com/, March 2012.

⑨LAP mentor. http://simbionix.com/simulators/lap-mentor/, March 2012.

⑩Laparoscopy™. http://www.immersion.com/, March 2012.

capacitance matrix algorithm (CMA) to solve the linear matrix system of (1) in real time rather than directly calculating $\boldsymbol{A}^{-1}$. In the preprocess, the reference boundary value problem is defined with the boundary conditions given by $\boldsymbol{A}\overline{\boldsymbol{Y}} + \boldsymbol{A}_0\overline{\boldsymbol{Y}_0} = 0$ (Fig.1), such that there is zero displacement ($\boldsymbol{\Gamma_u} = 0$) at any fixed boundary (i.e., contact between an organ and a bone, and zero traction ($\boldsymbol{\Gamma}_t = \boldsymbol{0}$) at any free boundary).

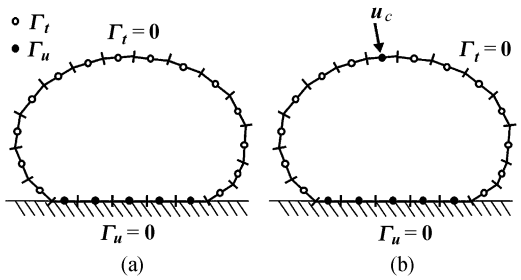

Fig.1. Boundary conditions for the boundary element method (BEM) are applied to boundary elements in (a) preprocess and (b) run-time process. ($\boldsymbol{\Gamma_u} = \boldsymbol{0}$: zero displacement, $\boldsymbol{\Gamma}_t = \boldsymbol{0}$: zero traction, $\boldsymbol{u}_c$: displacement vector from surgical instrument)

In the run-time process, the displacement boundary conditions ($\boldsymbol{u}_c$) are applied at the contact points between the liver and the surgical instrument models. Considering the change in the boundary conditions $\boldsymbol{S}$, the $\boldsymbol{A}$ matrix for a new set of boundary conditions can be represented from the precomputed $\boldsymbol{A}_0$ matrix by swapping simple s block columns. Using the ShermanMorrison-Woodbury formula, the relationship between $\boldsymbol{A}$ and $\boldsymbol{A}_0$ can be obtained as follows:

$$\boldsymbol{A}^{-1} = \boldsymbol{A}_0^{-1} - \boldsymbol{A}_0^{-1}(\overline{\boldsymbol{A}_0} - \boldsymbol{A}_0)\boldsymbol{I}_s\boldsymbol{C}^{-1}\boldsymbol{I}_s^{\mathrm{T}}\boldsymbol{A}_0^{-1}. \quad (3)$$

Hence, (2) can be represented by

$$\boldsymbol{Y} = \boldsymbol{A}^{-1}(\overline{\boldsymbol{A}}\,\overline{\boldsymbol{Y}}) = \boldsymbol{Y}^{(0)} + (\boldsymbol{I}_s + \Xi\boldsymbol{I}_s)C^{-1}\boldsymbol{I}_sY^{(0)} \quad (4)$$

where $\boldsymbol{I}_s$ is a $2n \times 2s$ submatrix of the identity matrix $\boldsymbol{Y}^{(0)} = [\boldsymbol{\Xi}(\boldsymbol{I} - \boldsymbol{I}_s\boldsymbol{I}_s^{\mathrm{T}}) - \boldsymbol{I}_s\boldsymbol{I}_s^{\mathrm{T}}]\overline{\boldsymbol{Y}}$. $\boldsymbol{C}(2s \times 2s)$ is known as the capacitance matrix and is given by $\boldsymbol{C} = -\boldsymbol{I}_s^{\mathrm{T}}\boldsymbol{\Xi}\boldsymbol{I}_s$. The Green's functions (GFs) $\boldsymbol{\Xi}$ are computed as $\boldsymbol{\Xi} = \boldsymbol{A}_0^{-1}\overline{\boldsymbol{A}_0}$. The solution $\boldsymbol{Y}$ for the tractions and displacements over the entire boundary can be obtained with the computational complexity of the inverse of the smaller capacitance matrix. Updating the deformation of the liver using the solution $\boldsymbol{Y}$, we can obtain the current position vector of the deformable object[12].

2.2 FEM Gallbladder Modeling

The gallbladder is a small pear-shaped organ that stores and concentrates bile produced by the liver. Bile enters and leaves the gallbladder via the cystic duct, travelling in a retrograde manner, when it is not needed for digestion. The gallbladder tends to have a flexible structure similar to a fluid-filled balloon. It is easier to represent the volumetric behavior of the gallbladder with FEM than with BEM, so we choose this physical-based modeling technique to describe its dynamic behavior.

As one of the continuum mechanics modeling methods, FEM is commonly used as the numerical technique to solve differential equations related to the equilibrium between stress and strain. While BEM is suitable for handling only the boundary of an object's surface, FEM is appropriate for describing a volumetric object at all the inner points. The discretized elements of the object, such as tetrahedral meshes, implicitly connect to each other and represent more realistic volumetric behaviors, such as whole-body movement, for balloon-like objects.

We generate a tetrahedral mesh model of the gallbladder by Delaunay tessellation[13] using the Visualization Toolkit (VTK)[11]. We focus only on modeling the dynamic behavior of the gallbladder by applying a simple FE elastic model, and we assume that only small deformations occur during surgical procedures. Assuming that strain and stress are in a linear elastic relationship, as described by Hooke's law, and that the total strain energy of the deformation is minimized over the domain boundary (a state of equilibrium), we can state that the static analysis of the object is governed by

$$\boldsymbol{K}\boldsymbol{u} = \boldsymbol{f}$$

or in the matrix formulation manner as

$$\begin{pmatrix} k_{11} & k_{12} & \cdots & k_{1n} \\ k_{21} & k_{22} & \cdots & k_{2n} \\ \vdots & \vdots & \ddots & \vdots \\ k_{3n\times 1} & k_{3n\times 2} & \cdots & k_{3n\times 3n} \end{pmatrix} \begin{pmatrix} u_1 \\ u_2 \\ \vdots \\ u_{3n} \end{pmatrix} = \begin{pmatrix} f_1 \\ f_2 \\ \vdots \\ f_{3n} \end{pmatrix}, \quad (5)$$

where $\boldsymbol{u}$ and $\boldsymbol{f}$ are $3n \times 1$ nodal displacement and force vectors, respectively. The $\boldsymbol{K}$ matrix is constructed by assembling the element stiffness matrices formed from the geometries of each tetrahedral element. More details are described in [2, 14]. With simple addition of mass inertia and energy dissipation terms, we can express the dynamic equations of the deformable model as

$$\boldsymbol{M}\ddot{\boldsymbol{u}} + C\dot{\boldsymbol{u}} + \boldsymbol{K}\boldsymbol{u} = \boldsymbol{f}, \quad (6)$$

where $\boldsymbol{M}$ and $\boldsymbol{C}$ denote the mass and damping, respectively, and $\ddot{\boldsymbol{u}}$ and $\dot{\boldsymbol{u}}$ represent the second and first derivative of $\boldsymbol{u}$ respectively. All matrices in (6) are symmetric, $3n \times 3n$, and sparse.

[11] Visualization toolkit (VTK). http://www.vtk.org, March 2012.

For resolving differential (6), there are several possible integration techniques[15], including explicit (e.g., the central difference method) and implicit approaches (e.g., Newmark's beta method to treat this problem by discretizing the time domain). While explicit methods require stable conditions and time interval constraints, implicit methods guarantee numerical stability independent of the time interval and mechanical properties such as Young's modulus[15]. Using this scheme, the dynamic behavior of a deformable object is expressed as follows:

$$\widetilde{\boldsymbol{K}}\boldsymbol{u}(t+\Delta t)=\tilde{\boldsymbol{f}}(t,t-\Delta t), \tag{7}$$

where $\widetilde{\boldsymbol{K}}$ and $\tilde{\boldsymbol{f}}$ are the effective tangential matrix and effective force vector, respectively. To obtain the solution of such a large sparse linear system, we need to use the preconditioned conjugate gradient (PCG) method[16]. This method is a widely used iterative linear solver for large symmetric sparse matrices that searches the direction vector and updates the solution vector. We set the user-specified tolerance to 10^{-8} and the maximum number of iterations to 20. In practice, the sequence of the solution vectors converges to 10 iterations.

2.3 Choosing Organ Model Physical Parameters

As mentioned, for a linear elastic material, the constitutive law is expressed by Hooke's law in tensor form:

$$\sigma_{ij}=\sum_{k.l}C_{ijkl}\varepsilon_{kl}. \tag{8}$$

The stress tensor $\boldsymbol{\sigma}$ contains six elements, and the six elements in the strain tensor $\boldsymbol{\varepsilon}$ represent the corresponding tensile and shear strain. Assuming that the two organs (the liver and gall bladder) consist of purely isotropic materials, (8) becomes $\boldsymbol{\sigma}=\boldsymbol{E}\boldsymbol{\varepsilon}$, meaning only a few parameters, such as Young's modulus and Poisson's ratio, need to be considered. Consequently, the results of (1) for BEM and (8) for FEM are obtained.

From data published in the literature, we have compiled the Young's moduli of human, bovine, corvine, and porcine liver and gallbladder (Table 1). It is necessary to choose mechanical parameters such as Young's modulus and Poisson's ratio using two physical-based modeling systems, FEM and BEM. Little experimental data exists concerning the Young's moduli of the human liver and gallbladder; we choose 170 kPa to model the human liver[17] and 2.3 kPa for the human gallbladder, the latter based on porcine data[18]. Most of the studies included in Table 1 assume that Poisson's ratio is below 0.49. We use 0.4 as the value for the liver and 0.45 for the gallbladder because the latter is a more rubber-like, soft tissue.

Table 1. List of Published Articles Providing Young's Moduli of Liver and Gallbladder

First Author	Experiment	Organ	Youngs Modulus (kPa)
Brown[19]	in vivo	Porcine liver	80.0
Carter[17]	in vivo	Human liver	170.0
Dan[20]	ex vivo	Bovine liver	10.0
Nava[21]	in vivo	Porcine liver	90.0
Ottensmeyer[22]	in vivo	Porcine liver	10.0∼15.0
Tay[23]	in vivo	Porcine liver	13.0
Schwarz[24]	in vivo	Cervine liver	2.5
Rosen[18]	in vivo	Porcine liver	7.3
Rosen[18]	in vivo	Porcine gallbladder	2.3

2.4 Connective Tissue Mass-Spring Modeling

Fibrous connective tissue exists between the liver and gallbladder. We approximate this tissue as a series of springs to model its mechanical behavior and implement surfaces between the springs for visualization. For each spring, one end is attached to the liver and the other is fixed to the gallbladder. The springs are updated during each frame of the simulation according to the corresponding deformations of the liver and gallbladder. If one endpoint of the spring moves while the liver/gallbladder deforms, the other end transfers the deformation to the other organ. Hooke's law is applied to the spring using the mass-spring method[2-3].

Entangled surfaces, such as membranes, are created using the following procedures for the visualization of connective tissue.

1) Candidate vertices on the gallbladder are selected at which to attach connective tissue springs. After translation of the gallbladder to the liver with a certain distance (e.g., 5 mm), the colliding vertices are checked.

2) Rays are casted from the selected vertices of the gallbladder to the liver, and intersecting points on the liver model are identified.

3) Connective tissue springs are created between the gallbladder vertices and the intersecting points on the liver (Fig.2(b)).

4) The end-points of each connective tissue line are concatenated with the gallbladder and liver models. Because the endpoints could be located at any position on the triangular or tetrahedral elements of the organ, barycentric mapping[25] is used to connect the endpoints and elements.

5) For each connective tissue spring, connective tissue surfaces are created from the four neighboring connective tissue springs as shown in Fig.2(a).

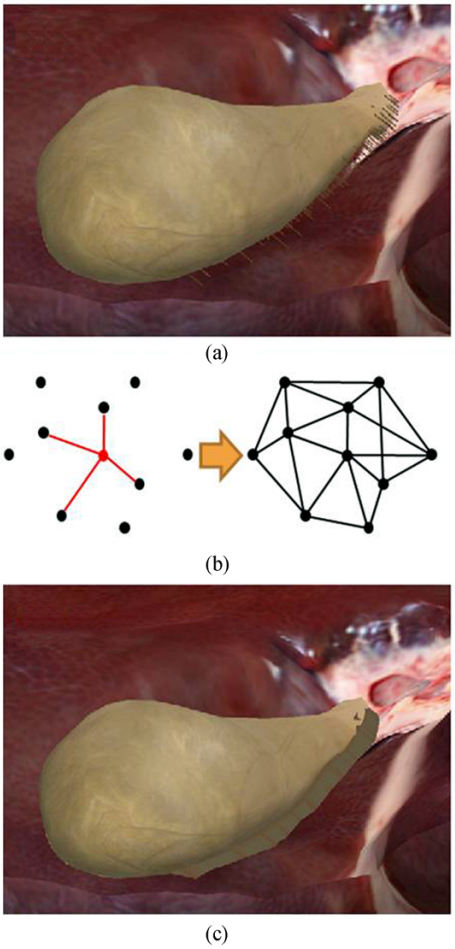

Fig.2. (a) Connective tissue springs. (b) Algorithm for modeling connective tissue. (c) Connective tissue modeling results. For each connective tissue spring, connective tissue surfaces were created from its four neighboring connective tissue springs. Each dot in (b) indicates one connective tissue spring.

6) Shading and texture mapping are carried out for each connective tissue surface.

2.5 Other Issues in Laparoscopic Surgery Simulation

2.5.1 Collision Checking

To simulate the interactions between the organs and the laparoscopic surgical instruments, it is necessary to check the collisions between the two mesh models[26]. A ray-tracing mesh-to-mesh collision detection algorithm[27] is applied to check the collisions between the liver/gallbladder and the left/right instrument. Collisions between the liver and the gallbladder are not considered because the connective tissue between them transfers deformations of one organ to the other. Self-collisions are also ignored because the deformations of each organ are small.

2.5.2 Grasping Simulation

To simulate gallbladder removal, grasping and pulling with graspers must be considered. Instead of computing the exact friction between the grasper tip and the organ model, we simplify the grasping simulation for real-time simulation. At each frame, the current and previous status of the graspers are checked. If closed, the graspers have a collision with an organ (and were previously open and had a collision) and grasp it. The grasping status is released when the tips are opened. This is also designed to simulate missed grasping that occurs when the graspers are moved more than a certain distance (e.g., 10 mm), to approximate the slippery nature of the gallbladder and to avoid excessive pulling.

2.5.3 Visual Effects for Burning and Removal of Connective Tissue

Texture mapping is conducted for all mesh models of the liver, gallbladder, and connective tissue. Special visual effects such as smoking and burning are implemented to provide a realistic simulation. When the cauterizer touches the organ, smoke is produced and the burned area of the organ turns black. To achieve this effect, prepared texture images of smoke are displayed with changing positions and decreasing alpha values. The smoke images are simultaneously augmented onto the simulation scene according to the user's manipulations. Next, the burning effect is implemented according to the method of Bruyns and Montgomery[28]. We improve their method by extending the blackening area, which includes contacting elements and their neighboring elements, by linearly decreasing the effect according to the distance from the original element. The blackened effect of each element is cumulative for repeated contact with the cauterizer.

In gallbladder removal surgery, connective tissues are cauterized while the gallbladder is pulled with graspers. Among the connective tissue surfaces in our simulation, elements colliding with the cauterizer hook are gradually eliminated, and the transparency contact time for each is incorporated into the model. The contacting connective tissue elements are deleted after gradually decreasing the transparency according to the contact time. The connective tissue spring that transfers deformations is eliminated once all of the corresponding connective tissue elements are removed.

2.5.4 Test-Bed Hardware and Haptic Rendering

A custom-designed haptic interface device (Fig.3) is developed for the simulation system, specifically designed to implement the four instrument position

degrees-of-freedom (DOF) of conventional laparoscopic surgery motion (yaw, pitch, roll, and translation) using a spherical robot system. The pitch (up-down motion) and yaw (left-right motion) joint are direct-drive configurations driven by brushed and geared DC motors. The translation motion joint is a wire-drive configuration using a BLDC motor without gearing for minimizing intrinsic friction. Conventional laparoscopic surgery instruments are loaded in the translation joint assembly, and haptic forces are calculated from the ray-based collision pairs[27]. The collision pairs between the instrument and liver models are directly obtained from the collision check. The computed reaction force vector is converted to the forces at each motor, and the appropriate feedback force is delivered while the user manipulates the haptic device.

Fig.3. Haptic interface device developed with integrated software for laparoscopic surgery simulation.

3 Results and Discussion

For a more realistic simulation of gallbladder removal, we approximate the behavior of the liver and the gallbladder using two physical-based methods, BEM and FEM. Although the liver and gallbladder have been modeled in various ways in related studies[2,29], in this section, we describe why BEM and FEM are suitable and effective alternative methods to do so.

For the liver model, global deformation is realistically and efficiently simulated in real time with BEM using the grasping simulation, as shown in Fig.4. To simulate the gallbladder behavior, FEM is used. Fig.5 shows that the influence of grasping and releasing is related to the overall behavior of the gallbladder. Figs.5(a)∼5(c) are snapshots of BEM simulations of the gallbladder and Figs.5(b) and 5(c) do not illustrate dynamic deformations. However, realistic dynamic motions of the gallbladder after being released from grasping can be seen in FEM simulations, as shown in Figs.5(e) and 5(f). Table 2 lists the computation time for BEM liver simulation. Avoiding direct computation of the inverse matrix ((2)), the BEM can calculate the deformation of the liver model with real-time rendering by pre-processing ((4)).

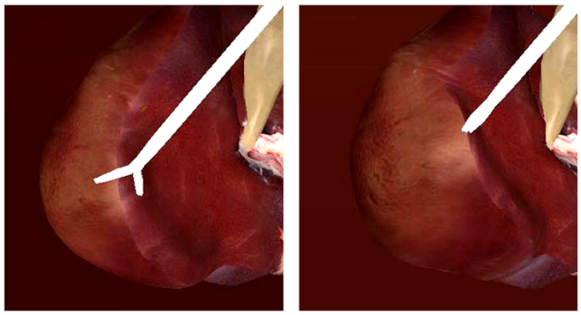

Fig.4. Snapshots of BEM deformation of the liver model during pulling by graspers.

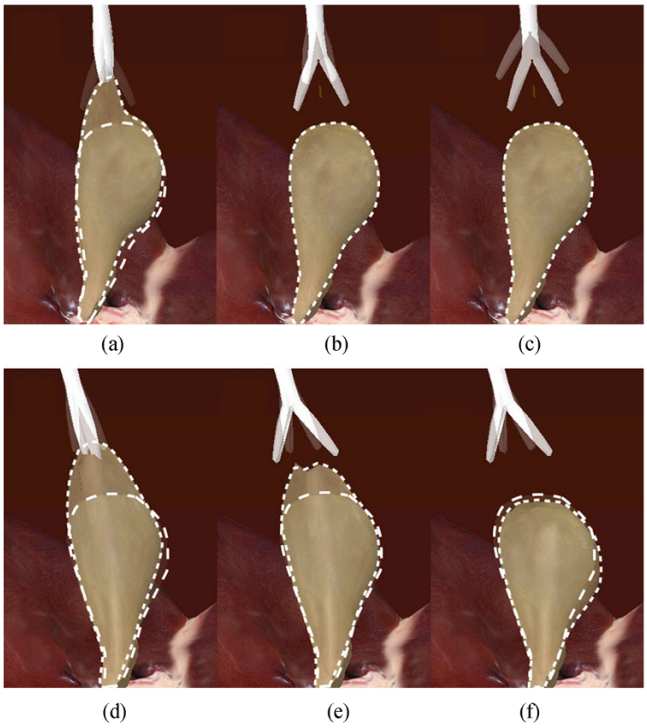

Fig.5. Comparison of BEM and FEM simulations of gallbladder deformation during release by the graspers. (a)∼(c) BEM deformation. (d)∼(f) FEM deformation. Each figure was captured with the same time interval.

Table 3 lists the computation time for the preprocess and the run-time process for FEM gallbladder simulation. In this case, most of the time is taken up by processing the time integration and solving the linear equations. The position of the virtual gallbladder is determined by the displacement induced by its dynamic

Table 2. Computation Time According to the Number of Nodes (BEM)

Number of Nodes	Pre-Process (ms)	Run-Time Process (ms)	
		Matrix Inversion ((2))	Global Deformation ((4))
95	108.6	3.7	0.361
296	2 886.8	44.2	2.979
752	46 597.3	351.1	5.566

Table 3. Computation Time According to the Number of Nodes (FEM)

Number of Nodes	Pre-Process (ms)	Run-Time Process (ms)		
		Boundary Condition	Time Integration and PCG Method	Global Deformation
310	1 241	440×10^{-3}	26.3	1.33
380	1 692	389×10^{-3}	33.0	0.62
469	2 194	526×10^{-3}	32.9	1.08
597	2 954	445×10^{-3}	35.1	1.08
769	3 990	506×10^{-3}	35.2	1.43
979	5 221	576×10^{-3}	38.3	1.86
1 272	6 891	490×10^{-3}	39.1	2.46
1 580	8 695	634×10^{-3}	46.4	3.15
1 980	11 004	629×10^{-3}	44.9	3.91
2 401	13 458	601×10^{-3}	45.0	4.88
2 865	16 142	440×10^{-3}	45.5	5.79

behavior, which is calculated by solving the linear system of the large sparse matrix from (7). Unlike BEM, the PCG method uses an iterative method to perform this inversion within a given user-specified threshold and a maximum number of iterations. FE-based real-time simulation of soft-tissue deformation is hindered by the large number of computations[10]; however, general-purpose graphic processing units (GPGPUs)⑫ are capable of handling many of these matrix calculations through parallel computing. In our study, by using GPGPUs, real-time simulation are achieved without incurring additional time cost, even for an increased number of nodes.

The results of the connective tissue modeling and other issues involved in the simulation are shown in Fig.6. Fig.6(a) shows the gallbladder being pulled by laparoscopic graspers. The connective tissues successfully transfer the deformations of the gallbladder to the liver (and vice versa) through the mass spring method described in Subsection 2.4. When the cauterizer contacts the organ model, it blackens the contacted area and produces the smoking effect shown in Fig.6(b). Fig.6(c) shows snapshots of the gallbladder removal simulation, in which the connective tissues are burned out with the cauterizer in the right hand, while the gallbladder is pulled by the graspers in the left hand. Trainees can be trained to manipulate two-handed laparoscopic instruments with our proposed system. The haptic interface device we developed for laparoscopic surgery training simulation is shown in Fig.3.

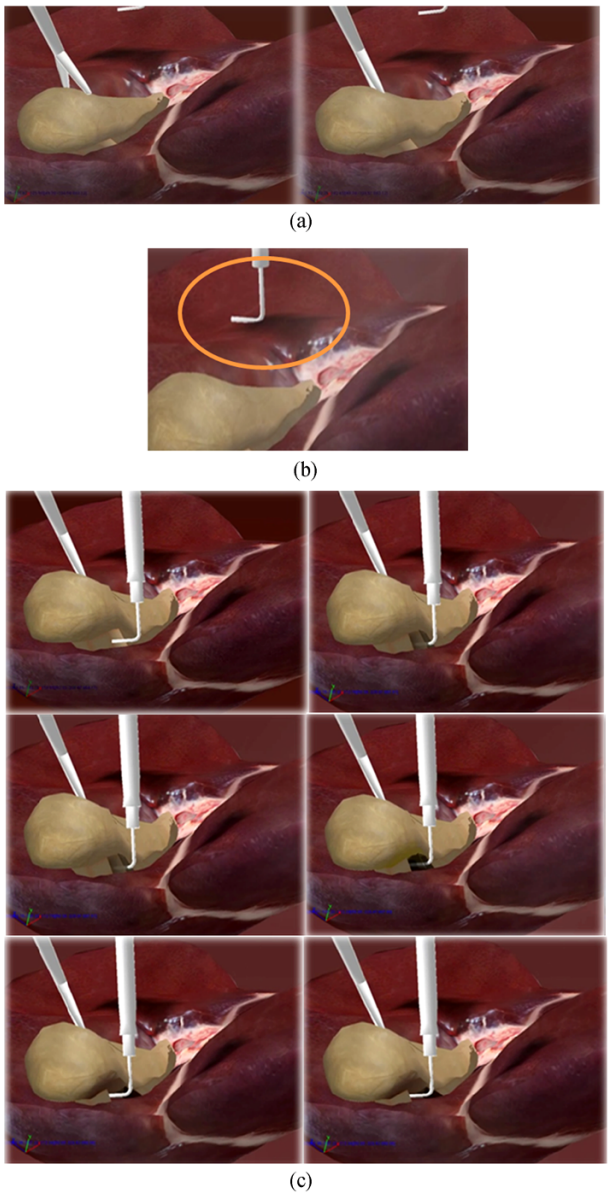

Fig.6. (a) Snapshots of a gallbladder grasping simulation in which the gallbladder is being pulled by laparoscopic graspers. (b) Example of burning simulation. When the cauterizer contacts the liver or the gallbladder, the contact area turns black and a smoke effect is produced. (c) Snapshots of the simulation of connective tissue removal.

4 Conclusions

We presented a hybrid modeling method for simulation of gallbladder removal that uses a combination of BEM and FEM. The BEM was used for liver deforma-

⑫CUDA. http://www.nvidia.com/cuda, March 2012.

tion, which is considered less dynamic, while FEM was used to model realistic dynamic behavior of the gallbladder. The results show that the proposed method is appropriate for simulating laparoscopic gallbladder removal. Other issues involved in developing the simulation system were also presented. In the future, we intend to investigate further gallbladder removal simulations such as clamping and cutting the biliary tract. We believe it will be possible to develop other surgical simulations using methods similar to those presented here. Such medical simulations include rectal surgery, prostate surgery, endoscopic surgery, arthroscopic surgery, and others.

References

[1] Allard J,Cotin S, Faure F *et al.* Sofa — An open source framework for medical simulation. In *Medicine Meets Virtual Reality 15*, Westwood J D, Haluck R S, Hoffman H M *et al.* (eds), 2007, pp.13-18.

[2] Meier U, López O, Monserrat C, Juan M C, Alcañiz M. Real-time deformablemodels for surgery simulation: A survey. *Computer Methods and Programs in Biomedicine*, 2005, 77(3): 183-197.

[3] Mosegaard J. Cardiac surgery simulation — Graphics hardware meets congenitalheart disease [Ph.D. Thesis]. Department of Computer Science, University of Aarhus, Denmark, 2006.

[4] Schijven M, Jakimowicz J. Virtual reality surgical laparoscopic simulators: How to choose. *Surgical Endoscopy*, 2003, 17(12): 1943-1950.

[5] Basafa E, Farahmand F, Vossoughi G. A non-linear mass-spring model for morerealistic and efficient simulation of soft tissues surgery. *Studies in Health Technologyand Informatics*, 2008, 132: 23-25.

[6] Cotin S, Delingette H, Ayache H. Real-time elastic deformations of soft tissues for surgery simulation. *IEEE Trans. Visualization and Computer Graphics*, 1999, 5(1): 62-73.

[7] Cover S A, Ezquerra N F, O'Brien J F *et al.* Interactively deformable models for surgery simulation. *IEEE Computer Graphics and Applications*, 1993, 13(6): 68-75.

[8] Basdogan C, Ho C H, Srinivasan M A. Virtual environments for medical training: Graphical and haptic simulation of laparoscopic common bile duct exploration. *Transactions on Mechatronics*, 2001, 6(3): 269-285.

[9] Samur E, Sedef M, Basdogan C, Avtan L, Duzgun O. A robotic indenter for minimally invasive measurement and characterization of soft tissue response. *Medical Image Analysis*, 2007, 11(4): 361-373.

[10] James D L, Pai D K. Multiresolution green's function methods for interactive simulation of large-scale elastostatic objects. *ACM Trans. Graphics*, 2003, 22(1): 47-82.

[11] Chen E, Marcus B. Force feedback for surgical simulation. *Proceedings of the IEEE*, 1998, 86(3): 524-537.

[12] Kim J, Janabi-Sharifi F, Kim J. A haptic interaction method using visual information and physically based modeling. *IEEE/ASME Trans. Mechatronics*, 2010, 15(4): 636-645.

[13] Guibas L, Knuth D, Sharir M. Randomized incremental construction of Delaunay and Voronoi diagram. *Algorithmica*, 1992, 7(1/6): 381-413.

[14] Mafi R, Sirouspour S, Mahdavikhah B S, Moody B, Elizeh K, Kinsman A, Nicolici N. A parallel computing platform for real-time haptic interaction with deformable bodies. *IEEE Trans. Haptics*, 2010, 3(3): 211-223.

[15] Bathe K J. Finite Element Procedures. New Jersey: Prentice-Hall, 1996.

[16] Shewchuk J R. An introduction to the conjugate gradient method without the agonizing pain. Technical Report, Carnegie Mellon University, USA, 1994.

[17] Carter F J, Frank T G, Davies P J *et al.* Biomechanical testing of intra-abdominal soft tissue. In *Proc. Int. Workshop. Soft Tissue Deformation and Tissue Palpation*, Oct. 1998.

[18] Rosen J, Brown J D, De S. Sinanan M, Hannaford B. Biomechanical properties of abdominal organs in vivo and postmortem under compression loads. *Journal of Biomechanical Engineering*, 2008, 130(2): 021020.

[19] Brown J D, Rosen J, Kim Y S *et al.* In-vivoand in-situ compressive properties of porcine abdominal soft tissues. In *Medicine Meets Virtual Reality 11*, Westwood J D, Hoffman H M, Mogel G T *et al.* (eds.), 2003, pp.26-32.

[20] Dan D. Caracterisation mecanique du foie humain en situation de choc [Ph.D. Thesis]. Universite Paris 7, France, 1999. (In French)

[21] Nava A, Mazza E, Kleinermann F, Avis N, McClure J. Determination of the mechanical properties of soft human tissues through aspiration experiments. In *Proc. the 6th MICCAI 2003*, Nov. 2003, pp.222-229.

[22] Ottensmeyer M P, Kerdok A E, Howe R D, Dawson S L. The effects of testing environment on the viscoelastic properties of soft tissues. In *Proc. ISMS 2004*, June 2004, pp.9-18.

[23] Tay B K, Kim J, Srinivasan M A. In vivo mechanical behavior of intraabdominal organs. *IEEE Trans. Biom. Eng.*, 2006, 53(11): 2129-2138.

[24] Schwartz J M, Denninger M, Rancourt D, Moisan C, Laurendeau D. Modelling liver tissue properties using a non-linear visco-elastic model for surgery simulation. *Medical Image Analysis*, 2005, 9(2): 103-112.

[25] Kim Y J, Park S H, Kim L H *et al.* Multi-model structure and mapping method of liver model. In *Proc Korean Society for Precision Engineering*, May 2010.

[26] Teschner M, Kimmerle S, Zachmann G *et al.* Collision detection for deformable objects. *Computer Graphics Forum*, 2005, 24(1): 61-81.

[27] Kim Y J, Koo S O, Lee D H *et al.* Mesh-to-mesh collision detection by ray tracing for medical simulation with deformable bodies. In *Proc. CyberWorlds*, Oct. 2010, pp.60-66.

[28] Bruyns C D, Montgomery K. Generalized interactions using virtual tools within the spring framework: Probing, piercing, cauterizing and ablating. *Studies in Health Technology and Informatics*, 2002, 85: 74-78.

[29] Luo X, Li W, Bird N, Chin S B, Hill N A, Johnson A G. On the mechanical behavior of the human biliary system. *World Journal of Gastroenterology*, 2007, 13(9): 1384-1392.

Youngjun Kim is a senior researcher in the Center for Bionics at Korea Institute of Science and Technology. He received his B.S. (2001), M.S. (2003), and Ph.D. (2009) degrees in mechanical engineering from Seoul National University, Korea. His research interests include 3D medical imaging, medical simulation and computer aided surgery.

Dongjune Chang received his B.S degree in 2010 with a double major in mechanical engineering and mathematical sciences from Korea Advanced Institute of Science and Technology, Daejeon. He is currently working as a researcher in Dongbu Robot Co., Ltd, Bucheon. His current research interests include physical modeling, physical human robot interactions and tremor suppression.

Jungsik Kim received the B.S. degree in mechanical engineering from Inha University, Incheon, in 2006, and the M.S. degree in mechanical engineering from Korea Advanced Institute of Science and Technology (KAIST), in 2008. He is currently working toward the Ph.D. degree in mechanical engineering at KAIST. His current research interests include biomicromanipulation, telerobotics, and mechanical characterization of soft tissue.

Sehyung Park is a principal researcher in the Center for Bionics at Korea Institute of Science and Technology. His research interests include geometric modeling, human computer interface, medical simulation and computer aided surgery. Park received a BS degree from Seoul National University in mechanical design and production engineering and an M.S. degree in mechanical engineering from Cornell University, and a Ph.D. degree in mechanical engineering from Korea Advanced Institute of Science and Technology.